

# Reducing pervasive false positive identical-by-descent segments detected by large-scale pedigree analysis

Eric Y. Durand<sup>1,\*</sup>, Nicholas Eriksson<sup>1</sup>, and Cory Y. McLean<sup>1,\*†</sup>

<sup>1</sup>23andMe, Inc., 1390 Shorebird Way, Mountain View, CA, 94110, USA

\*These authors contributed equally to this work.

†Correspondence should be addressed to C.Y.M. (cmclean@23andme.com).

07/15/22

## Contents

Main text . . . . .	2
Figures . . . . .	5
Supplementary Methods . . . . .	7
Supplementary Figures . . . . .	12
Supplementary Tables . . . . .	23
References . . . . .	25

## Abstract

**Analysis of genomic segments shared identical-by-descent (IBD) between individuals is fundamental to many genetic applications, but IBD detection accuracy in non-simulated data is largely unknown. Using 25,432 genotyped European individuals, and exploiting known familial relationships in 2,952 father-mother-child trios contained therein, we identify a false positive rate over 67% for short (2-4 centiMorgan) segments. We introduce a novel, computationally-efficient, haplotype-based metric that enables accurate IBD detection on population-scale datasets.**

Detecting the presence and distribution of IBD segments between individuals is fundamental to long-range phasing<sup>1</sup>, disease gene discovery<sup>2,3</sup>, heritability estimation<sup>4,5</sup>, demographic history inference<sup>6,7,8</sup>, identifying regions under natural selection<sup>9,10</sup>, and other genetic applications<sup>11</sup>. IBD detection accuracy is typically assessed on simulated data, as true IBD segments can then be known precisely<sup>9,12,13,14</sup>. However, accurate simulation of population demography is difficult<sup>11</sup>, and simulation parameters directly affect the estimated precision and recall of IBD detection algorithms.

Most existing IBD detection algorithms scale quadratically with input sample sizes and are thus not suitable for IBD detection in large datasets (reviewed in ref. 11). In this study, GERMLINE<sup>7,13</sup> was used to detect IBD segments since it decouples genotype phasing from IBD detection, a necessity for population-scale datasets. Briefly, GERMLINE identifies seeds of phased haplotype matches to begin candidate IBD segments, and extends seeds either by haplotype or diplotype matching with parameters chosen to identify IBD segments in the presence of genotype and switch errors<sup>7,13</sup>.

To analyze IBD detection accuracy on real data, we examined IBD segments detected in a cohort of 25,432 individuals of European ancestry that includes 2,952 distinct father-mother-child trios (**Supplementary Methods**). By focusing specifically on segments reported between a trio child and an individual who is not a parent of that child (henceforth called “child-other” segments), we can quantify IBD accuracy: by the definition of IBD, if a child-other segment is true, at least one of the child’s parents must also share a segment IBD with the individual (henceforth called “parent-other” segments) that encompasses the child-other segment.

A total of 13,307,562 child-other segments were detected on chromosome 21, only 14% of which were encompassed by a parent-other segment (**Fig. 1a, Supplementary Fig. 1**). Another 25% of child-other segments have a partial parent-other segment in which at least one segment end is truncated (**Fig. 1a**). Segment ends imply the presence of opposite homozygote genotypes between the individuals. Opposite homozygote sites that terminate a parent-other segment exclude the possibility of child-other IBD at those sites. To determine whether truncated segment ends represented false child-other IBD or genotype error in parent-other regions, Illumina GenCall scores were examined at the opposite homozygote sites truncating 128,656 randomly-selected partial parent-other segments. Considering GenCall scores of  $\geq 0.7$  as confident genotype calls<sup>15</sup>, over 95% of opposite homozygote sites analyzed (122,364/128,656) have confident genotype calls in both the parent and other individual, indicating that the vast majority of disagreements between child-other and parent-other segments represent false positive IBD in the child rather than false negative IBD in the parent (**Fig. 1b**).

Finally, the majority (61%) of child-other segments have no corresponding parent-other segment (**Fig. 1a**). The relative representation of false positive child-other segments and false negative parent-other segments was quantified using the number of parent-other opposite homozygotes seen in the region (**Supplementary Fig. 1c**). Nearly 98% of these child-other segments have at least one opposite homozygote site in the parent (**Fig. 1c**), leading to a conservative estimate of false positive child-other segments of over 97% in this subset (**Supplementary Methods**).

The unexpectedly small number of child-other segments that are fully spanned by a corresponding parent-other segment motivated an analysis of the relationship between segment length and segment overlap. Segment overlap between parent and child was calculated based on the fraction of sites in the child-other segment (**Supplementary Fig. 1**). **Fig. 2a** shows the average segment overlap for segments segregated by genetic and physical lengths. While segments longer than 6 centiMorgans (cM) generally show a high degree of overlap, the average overlap drops rapidly as segment length is reduced (**Fig. 2a**).

IBD accuracy was estimated by considering child-other segments with substantial parent-other segment overlap as true IBD. Because precise determination of IBD endpoints from genotype data is difficult<sup>14</sup>, a threshold of 80% segment overlap was used to classify a segment as true IBD. Using this criterion, more than 67% of all reported segments shorter than 4 cM are false positive child segments (**Fig. 2b**, **Supplementary Fig. 5**). Notably, over 98% of all reported child-other segments are shorter than 4 cM (**Supplementary Fig. 6**). Poor precision in short segments is due to the allowance of diplotype-only matches within the IBD detection algorithm (**Supplementary Table 1**) but is necessary for detection of long segments due to imperfect haplotype phasing<sup>7</sup>.

IBD is fundamentally a property of haplotypes, not diplotypes. Consequently, true IBD should appear consistent with haplotype matches, modulo expected genotype and switch errors. We introduce HaploScore as a measure of haplotype IBD likelihood: given a genotype error rate per site  $\epsilon$  and a switch error rate per site  $\sigma$ , the HaploScore for a candidate IBD segment  $S$  is

$$\text{HaploScore}(S) = \frac{1}{|S|} \left( \frac{n_g}{\epsilon} + \frac{n_s}{\sigma} \right) \quad (1)$$

where  $|S|$  is the number of genotyped sites in  $S$  and  $n_g$  and  $n_s$  are the number of genotype and switch errors, respectively, that together minimize the score while reconciling the segment as matching across a single haplotype in both individuals. Genotype and switch error rates per site were estimated from the data to be  $\epsilon = 0.0075$  and  $\sigma = 0.003$  (**Supplementary Methods**).

HaploScore effectively discriminates between true and false IBD at all segment lengths examined (**Fig. 2c**). Power increases as segment length increases (**Fig. 2d**), owing in part to the enrichment of false positives in short segments (**Supplementary Fig. 5**). However, since HaploScore provides a way to rank segments, the tradeoff between precision and recall can be tuned to the particular application (**Supplementary Fig. 7**).

HaploScore depends only on the relative rates of genotype and switch errors. Consequently, it is robust to a wide variety of estimates of each error rate (**Supplementary Fig. 8**). Moreover, HaploScore can be computed efficiently using dynamic programming (in  $O(|S|)$  time per segment, **Supplementary Methods**). Generality of the method was confirmed by examining performance when using different segment overlap thresholds to define true IBD (**Supplementary Fig. 9**) and by applying the method to IBD data on another chromosome (**Supplementary Fig. 10**).

Our results identify a surprisingly high rate of false positives in diplotype-based hash-and-extend IBD detection methods when applied to non-simulated data. We introduce a haplotype-based metric that effectively discriminates between true and false reported IBD segments. The metric is useful for all IBD segment applications, can be applied to existing genotyping- and sequencing-based IBD segments as an efficient post-processing step, and enables accurate IBD detection on population-scale datasets.

Python code implementing HaploScore filtering is freely available (<https://github.com/23andMe/ibd>).

## **Acknowledgments**

We thank the customers of 23andMe who contributed the genetic data that made this research possible and are grateful to the employees of 23andMe for creating and supporting the resources necessary for this research. We also thank members of the 23andMe research team for insightful comments.

## **Author Contributions**

C.Y.M., E.Y.D., and N.E. conceived and designed experiments. E.Y.D. and C.Y.M. performed experiments and analyzed the data. C.Y.M. wrote the paper with contributions from E.Y.D. and N.E.

## **Competing financial interests**

E.Y.D., N.E., and C.Y.M. are employees of and own stock options in 23andMe, Inc.

## Figures

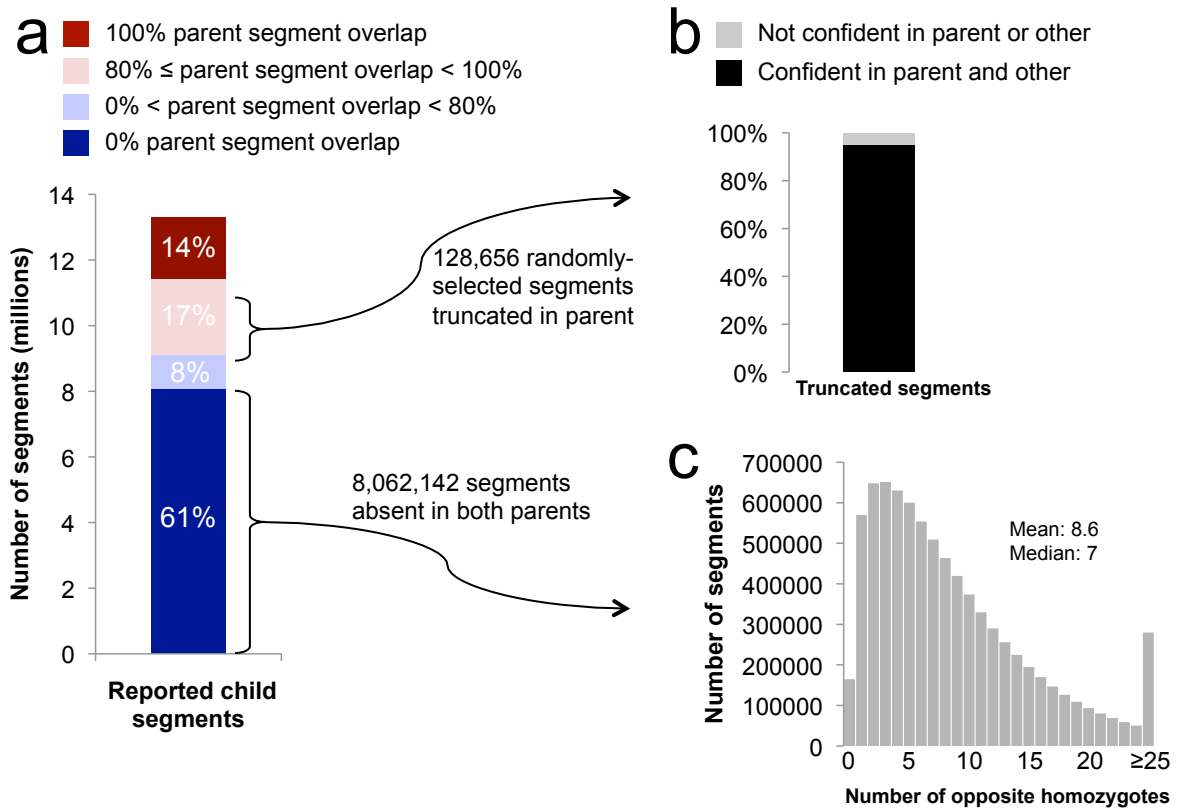


**Figure 1:** Analysis of child-other segments in parents. (a) The majority of child-other segments are not detected in either parent. Parent segment overlap is calculated as the percentage of sites in the child-other segment that are included in the parent-other segment. (b) Truncation points for parent-other segments are nearly always confidently-genotyped opposite homozygote sites, consistent with false positive IBD in the child. The opposite homozygote site causing truncation of the parent-other segment was examined in a randomly-selected subset of all 3,371,616 segments with partial parent overlap. (c) Child-other segments entirely absent in parents contain many parent-other opposite homozygotes in the region, also consistent with false positive IBD in the child. For each child-other segment absent in both parents, the number of opposite homozygote sites present between the parent and the other individual at that segment location is calculated separately for each parent, and the smaller is chosen as the number of opposite homozygotes in the region.

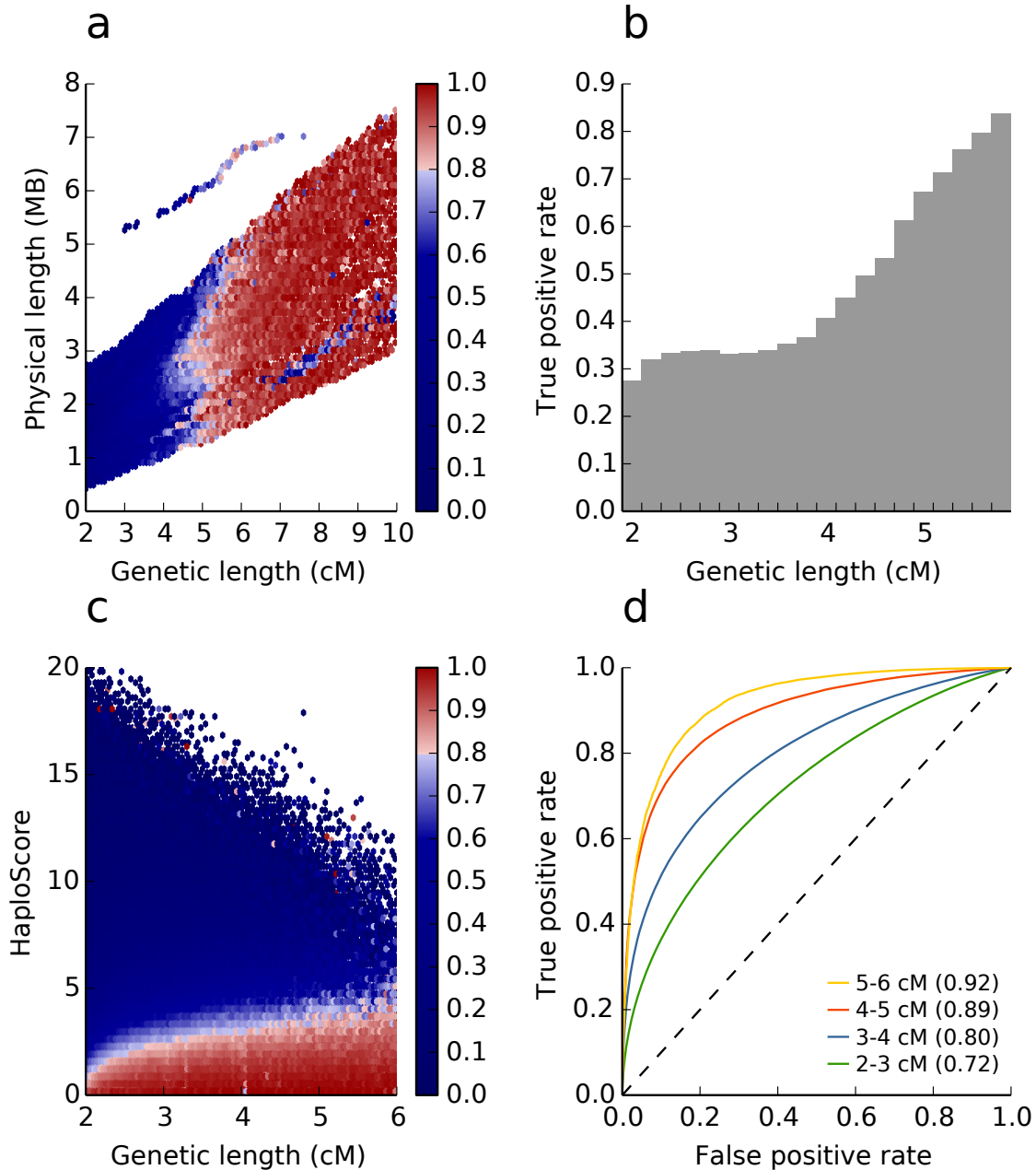


**Figure 2:** Improving detection of true IBD segments using HaploScore. (a) Heat map of the average segment overlap in child-other segments, binned by two measures of segment length. For each child-other segment, the fraction of the segment also reported as an IBD segment between the parent and the other individual is calculated. Shown in each bin is the mean of the segment fractions calculated for all segments in the bin. (b) The fraction of child-other segments that are true IBD as a function of segment length. True IBD segments are defined as having at least 80% of their sites encompassed by a parent-other segment. (c) Heat map of the mean fraction of reported IBD segments found in parents, binned by segment genetic length and HaploScore. Calculations are performed as in (a). (d) Receiver operating characteristic for reported IBD segments of various lengths, discriminating by HaploScore. True IBD is defined as in (b). The dashed black line indicates the no-discrimination line. The area under each curve is parenthesized in its legend entry.

# Supplementary Methods

## Cohort description

The cohort analyzed is composed of a total of 25,432 customers of 23andMe, Inc., a personal genetics company, who had been genotyped on the Illumina HumanOmniExpress+ BeadChip as part of the 23andMe Personal Genome Service. The chip contains roughly 1,000,000 sites genome-wide<sup>16</sup>. Individuals were selected for having > 97% European ancestry as described previously<sup>16</sup>. The cohort includes 2,952 distinct father-mother-child trios identified by identity-by-descent (IBD) sharing<sup>17</sup>. Parent-child relationships were defined as having at least 85% of the genetic length of the genome shared on at least one haplotype and no more than 10% of the genetic length of the genome shared on both haplotypes. Parent-parent relationships were defined as having at most 20% of the genetic length of the genome shared on at least one haplotype.

## IBD detection

Genotypes of all individuals included in the study were phased using BEAGLE<sup>18</sup> version 3.3.1 in batches of 8,000–9,000 individuals as described previously<sup>16</sup>. In each batch, we excluded sites with minor allele frequency < 0.001, Hardy-Weinberg equilibrium  $P < 10^{-20}$ , call rate < 95%, or large allele frequency discrepancies compared to the 1000 Genomes Project reference data. Input haplotypes were restricted to sites present in the intersection of all batch-filtered sites, and resulted in 12,881 sites on chromosome 21 and 48,372 sites on chromosome 10.

For each of the 2,952 trio children, candidate IBD segments were calculated between the child and all 25,429 other individuals who were not the parents of that child. For each of the 5,904 ( $= 2 \times 2,952$ ) trio parents, candidate IBD segments were calculated between the parent and all 25,430 other individuals who were not the child of that parent. All candidate IBD segments were calculated using the GERMLINE<sup>13</sup> algorithm with the parameters `-bits 100 -err_hom 2 -err_het 0 -w_extend -min_m 2 -map <geneticmap>`, corresponding to the empirical genotype and switch error rates of the data (see **HaploScore parameter estimation** below). The genetic map used was generated by the Phase II HapMap<sup>19</sup> and lifted over to NCBI Build GRCh37 coordinates using the UCSC Genome Browser<sup>20</sup> liftOver tool (available at [http://hapmap.ncbi.nlm.nih.gov/downloads/recombination/2011-01\\_phaseII\\_B37/genetic\\_map\\_HapMapII\\_GRCh37.tar.gz](http://hapmap.ncbi.nlm.nih.gov/downloads/recombination/2011-01_phaseII_B37/genetic_map_HapMapII_GRCh37.tar.gz)). To omit clearly artifactual candidate IBD segments arising from sequence assembly gaps and platform effects, candidate segments were filtered to omit segments with a site density (measured in sites/cM) in the lowest 10% of all 1 cM windows on the chromosome. All remaining candidate IBD segments were retained.

## Estimating false positive child IBD rate in segments with no corresponding parent segment

Child-other segments that have no corresponding parent segment (**Supplementary Fig. 1c**) were analyzed to determine whether they represented false positive child-other segments, or false negative parent-other segments. Given a 95% accuracy rate for parent-other opposite homozygote sites (**Fig. 1b**), we calculate the probability that a region containing  $N$  opposite homozygote sites is actually a false negative parent-other IBD segment as  $(1 - 0.95)^N$ . The expected fraction of false negative parent-other segments is 0.0242, and thus the fraction of false positive child-other segments is 0.9758. This likely represents a conservative (i.e. low) estimate of false positive child-other segments, as segments with no opposite homozygote sites can still be not shared IBD.

## Haplotype and diplotype window contributions to segment detection and accuracy

With perfect genotype phasing, IBD detection would only need to examine haplotypes. However, switch errors occur at an appreciable frequency in statistically-phased data (**Supplementary Fig. 2**). Examination of only haplotypes in the presence of switch errors reduces power to detect IBD<sup>14</sup>.

Detection of child-other segments with no corresponding parent-other segment could arise from haplotype matching between the child and the other individual, but a switch error in the parent causing the corresponding haplotype to not match between the parent and the other individual. To examine whether switch errors contribute to the large discrepancies seen between child-other and parent-other IBD segments, we trio-phased all 2,952 trios using the laws of Mendelian inheritance and then performed IBD detection as described above. Trio-phasing ensures that children and parents are phased essentially perfectly, eliminating haplotype discrepancies between parent and child as contributing to segment discrepancies. The number and accuracy of child-other segments using trio-phased data is nearly identical to that of BEAGLE-phased data, showing that parent-child haplotype discrepancies contribute a negligible amount toward discrepant segments (**Supplementary Fig. 3**).

Alternatively, child-other segments with no corresponding parent-other segment could be false reported IBD between the child and the other individual due to overly permissive diplotype matching. To examine this possibility, we analyzed each full 100-site window in all 13,307,562 child-other segments (63,542,380 total windows) to see whether the window satisfied the diplotype match criteria and the haplotype match criteria between the child and the other individual and between the parent and the other individual. We segregate analysis by windows contained within corresponding parent-other segments (likely true IBD) and windows that are not contained within corresponding parent-other segments (false IBD). The diplotype match criteria are satisfied in the child in 97.6% of windows contained within parent-other segments (**Supplementary Table 1a**) and in 97.5% of windows not contained within parent-other segments (**Supplementary Table 1b**). Roughly 67.7% of windows contained within both child-other and parent-other segments satisfy the haplotype match criteria for IBD in the child (**Supplementary Table 1a**), consistent with true IBD given the empirical switch error rate and window size (**Supplementary Fig. 2**). In contrast, only 44.2% of windows not contained within a parent-other segment satisfy the haplotype match criteria for IBD in the child (**Supplementary Table 1b**), a substantial reduction (binomial  $P < 10^{-300}$ ).

The substantial reduction in windows matching haplotypes in regions of false IBD suggest a haplotype-based metric that is robust to switch errors could improve precision of reported IBD without the loss of recall incurred by haplotype-only IBD detection mechanisms.

## HaploScore description and computational complexity

HaploScore provides a metric by which to rank the likelihood that a stretch of DNA is inherited IBD between two individuals or not. We model genotype and switch errors as independent Bernoulli processes that occur at each site with probability  $\epsilon$  and  $\sigma$ , respectively. For a stretch of DNA containing  $L$  genotyped sites, the expected number of genotype errors,  $E[n_g]$ , within the stretch is  $\epsilon L$  and the expected number of switch errors,  $E[n_s]$ , is  $\sigma L$ . Consequently, the expected value of  $\frac{1}{L} \left( \frac{n_g}{\epsilon} + \frac{n_s}{\sigma} \right)$  is constant for all segment lengths:

$$\begin{aligned} E \left[ \frac{1}{L} \left( \frac{n_g}{\epsilon} + \frac{n_s}{\sigma} \right) \right] &= \frac{1}{L} \left( \frac{E[n_g]}{\epsilon} + \frac{E[n_s]}{\sigma} \right) \\ &= \frac{1}{L} \left( \frac{\epsilon L}{\epsilon} + \frac{\sigma L}{\sigma} \right) \\ &= 2 \end{aligned}$$



The HaploScore for a candidate IBD segment  $S$  is

$$\text{HaploScore}(S) = \frac{1}{|S|} \left( \frac{n_g}{\epsilon} + \frac{n_s}{\sigma} \right) \quad (2)$$

where  $|S|$  is the number of genotyped sites in  $S$  and  $n_g$  and  $n_s$  are the number of genotype and switch errors, respectively, that together minimize the score while reconciling the segment as matching across a single haplotype in both individuals.

Finding the HaploScore (i.e. the optimal values of  $n_g$  and  $n_s$  subject to the constraints) can be viewed as finding the minimum-cost path through the directed acyclic graph (DAG) described below (**Supplementary Fig. 4**).

Let  $G$  be a DAG with a single source node and a single sink node. Between the source and the sink, the graph has  $|S|$  levels, one per genotyped site in segment  $S$ . Each of these  $|S|$  levels has four nodes, one for each possible haplotype configuration. Each node in level  $l$  has four outgoing directed edges, one to each node in level  $l + 1$ . Below, we use the same notation for nodes (respectively, edges) and their weights.

At any level  $l$ , let  $h_l^{(i,j)}$ ,  $i, j \in 1, 2$  denote the four possible haplotype configurations of an IBD match. The nodes are weighted as follows:

$$h_l^{(i,j)} = \begin{cases} 0 & \text{if haplotype } i \text{ in first individual matches haplotype } j \text{ in second individual} \\ 1/\epsilon & \text{otherwise} \end{cases} \quad (3)$$

Let  $e_l^{(i,j),(u,v)}$  denote the edge between nodes  $h_l^{(i,j)}$  and  $h_{l+1}^{(u,v)}$ . The edges are weighted as follows:

$$e_l^{(i,j),(u,v)} = \begin{cases} 0 & \text{if } i = u \text{ and } j = v \\ 1/\sigma & \text{if } i = u \text{ and } j \neq v \\ 1/\sigma & \text{if } i \neq u \text{ and } j = v \\ 2/\sigma & \text{if } i \neq u \text{ and } j \neq v \end{cases} \quad (4)$$

The weights of the four edges from the source node to the nodes in the first level, as well as the weights from the nodes in level  $|S|$  to the sink node, are set to 0. The cost of a path in  $G$  is defined as the sum of the weights of the edges and nodes it traverses.

HaploScore( $S$ ) is equal to the smallest of all path costs from the source to the sink. It can be efficiently computed using dynamic programming by noting that the smallest cost from the source to level  $l + 1$  in the graph can easily be inferred from the smallest cost from the source to level  $l$ . Let  $C_l$  denote the smallest cost from the source to level  $l$ . Then,

$$C_{l+1} = C_l + \min_{i,j,u,v} \left( e_l^{(i,j),(u,v)} + h_{l+1}^{(i,j)} \right) \quad (5)$$

The above equation clearly shows that computing HaploScore( $S$ ) involves 16 comparisons at each genotyped site in  $S$ . Thus, the complexity of computing HaploScore( $S$ ) is at most  $16|S|$ . Performance can be further improved when filtering by HaploScore by terminating computation as soon as a segment's HaploScore becomes too high to satisfy the maximum value threshold.

## HaploScore parameter estimation

HaploScore uses two parameters, the genotyping error rate per site  $\epsilon$  and the switch error rate per site  $\sigma$ . To estimate the empirical switch error rate per site, we trio-phased all 2,952 trios using the laws of Mendelian inheritance and compared the results for the trio children to their BEAGLE-phased haplotypes, assuming that the trio-phased haplotypes represent the true phase. The average per-site switch error rate ranges

from 0.0019 (on chromosome 6) to 0.0043 (on chromosome 19) but deviates only modestly from a constant rate on each chromosome (**Supplementary Fig. 2**). Analyses of genotyping chip accuracy<sup>21</sup> and internal comparisons between genotype and whole-genome sequencing data verify that the genotyping error rate is < 1% (not shown).

## HaploScore filtering thresholds

HaploScore can be used to filter out spurious segments reported by an IBD detection algorithm as an efficient post-processing step. Ideally, because HaploScore should be constant for all true IBD segments regardless of segment length, a single HaploScore value threshold should suffice. However, in practice the reduced power to detect short segments requires more stringent HaploScore threshold values to achieve a similar positive predictive value as for longer segments (**Fig. 2c, Supplementary Fig. 7a**). We generated a matrix of thresholds in the following manner: we binned segments by length in 0.1 cM increments from 2 cM to 10 cM. In each length bin, we segregated segments by their segment overlap into 100 equally-sized overlap bins. The score threshold in each overlap bin was initially set to be the average HaploScore of all segments within the bin. To ensure monotonicity, the score threshold was then taken to be the maximum of the scores in all bins of equal or higher overlap at that segment length. Resulting segment counts after filtering at multiple average overlap thresholds are shown in **Supplementary Fig. 7b**.

## Robustness of results to HaploScore parameter variation

HaploScore is a function of both the genotype error rate  $\epsilon$  and the switch error rate  $\sigma$ , but only the ratio of the two parameters affects the behavior of the score. In order to assess the robustness of HaploScore to varying parameters, we performed a grid search in which we varied  $\sigma$ , leaving  $\epsilon$  fixed at 0.0075. We varied  $\sigma$  from  $\epsilon/1000$  to  $10\epsilon$  and computed the area under the receiver operating characteristic curve (AUC) at each grid point. **Supplementary Fig. 8** shows the AUC as a function of the score parameters.

Except where otherwise noted, true IBD segments were defined as child-other segments that have at least 80% parent-other segment overlap. To assess the robustness of HaploScore to different true IBD definitions, we performed a grid search in which we varied the definition of true IBD from 10% to 100% parent-other segment overlap in increments of 10% and computed the AUC at each grid point. **Supplementary Fig. 9** shows the AUC as a function of the true IBD definition.

To confirm that the results presented are not due to particular genomic features of chromosome 21, we analyzed chromosome 10 using the same parameters ( $\epsilon = 0.0075$ ,  $\sigma = 0.003$ , 80% segment overlap defines true IBD). Results are qualitatively similar to chromosome 21 (**Supplementary Fig. 10**). We also examined segments in a subset of all individuals on all autosomes and observed no substantial deviations in performance (not shown).

## Logarithm of Odds (LOD) segment scoring

In this section, we describe an alternative scoring for potential IBD segments that is similar in spirit to the LOD score used in RefinedIBD<sup>14</sup>. Specifically, for a given segment  $S$  shared between two individuals  $i_1$  and  $i_2$ , we compute LODscore as follows:

$$\text{LODscore}(S) = \log \frac{\Pr(G_{obs1}^{(S)}, G_{obs2}^{(S)} | \text{IBD})}{\Pr(G_{obs1}^{(S)}, G_{obs2}^{(S)} | \text{no IBD})} \quad (6)$$

where  $G_{obs1}^{(S)}$  (resp.  $G_{obs2}^{(S)}$ ) are the genotypes of individual  $i_1$  (resp.  $i_2$ ) over segment  $S$ , and  $\Pr(G_{obs1}^{(S)}, G_{obs2}^{(S)} | \text{IBD})$

(resp.  $Pr(G_{obs1}^{(S)}, G_{obs2}^{(S)} | \text{no IBD})$ ) is the pseudo-likelihood of observing  $G_{obs1}^{(S)}$  and  $G_{obs2}^{(S)}$  conditioned on individuals  $i_1$  and  $i_2$  being IBD over segment  $S$  (resp. not being IBD).

The pseudo-likelihood is computed as:

$$Pr(G_{obs1}^{(s)}, G_{obs2}^{(s)} | \text{IBD}, \epsilon) = \prod_{i=1}^{\#s} \sum_{G_{true1}^{(i)}} \sum_{G_{true2}^{(i)}} Pr(G_{true1}^{(i)}, G_{true2}^{(i)} | \text{IBD}) Pr(G_{true1}^{(i)} | G_{obs1}^{(i)}, \epsilon) Pr(G_{true2}^{(i)} | G_{obs2}^{(i)}, \epsilon)$$

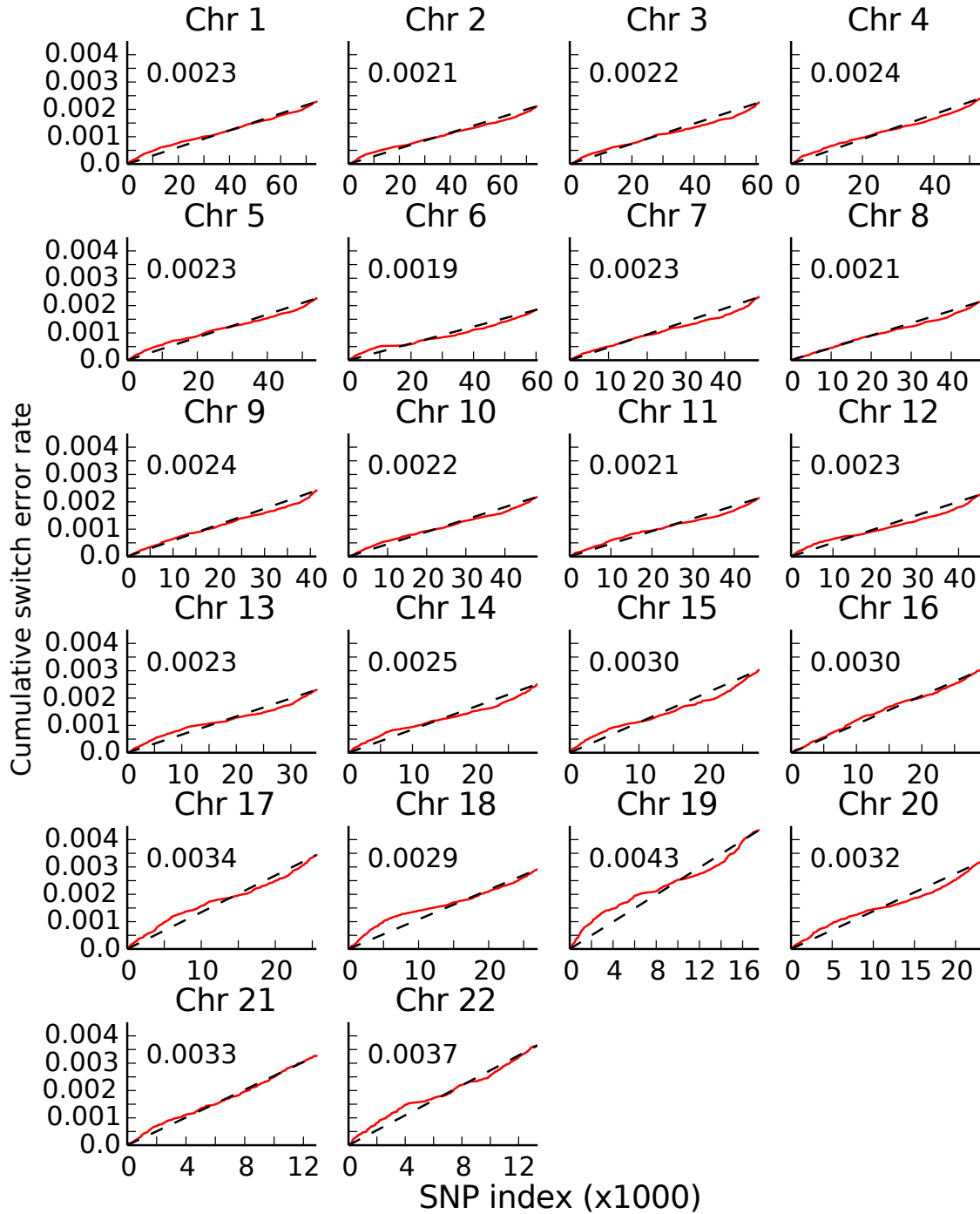
where  $\epsilon$  is the genotyping error rate,  $\#s$  is the number of markers in the IBD segment, and  $G_{truej}^{(i)}$  is the true genotype in individual  $j$  at position  $i$ . The probability of genotypes  $(G_{true1}^{(i)}, G_{true2}^{(i)})$  as a function of the IBD state (0, 1 or 2 alleles IBD at position  $i$ ) is given in **Supplementary Table 2**. We note that **Supplementary Table 2** was derived elsewhere<sup>9</sup>. The probability of observing a genotype given the true genotype and the genotyping error rate is given in **Supplementary Table 3**. Two genotypes are considered IBD if they either share one or two alleles IBD (IBD1 and IBD2 in **Supplementary Table 3**), and we give equal prior probabilities to the two configurations.

We assessed the performance of LODscore by computing its AUC for various segment sizes. We note that even though the LODscore has power to filter out false IBD segments, its AUC is generally lower than the HaploScore detailed in the main text (**Supplementary Fig. 11**). Reasons for the lower power of LODscore may arise in part from two issues: 1) LODscore assumes each site is independent and thus ignores correlation between adjacent markers, and 2) LODscore ignores available phase information. Both issues could be alleviated by explicitly incorporating linkage disequilibrium between adjacent sites and switch errors into the model. However, because of the strong performance of HaploScore, we leave this to future work.

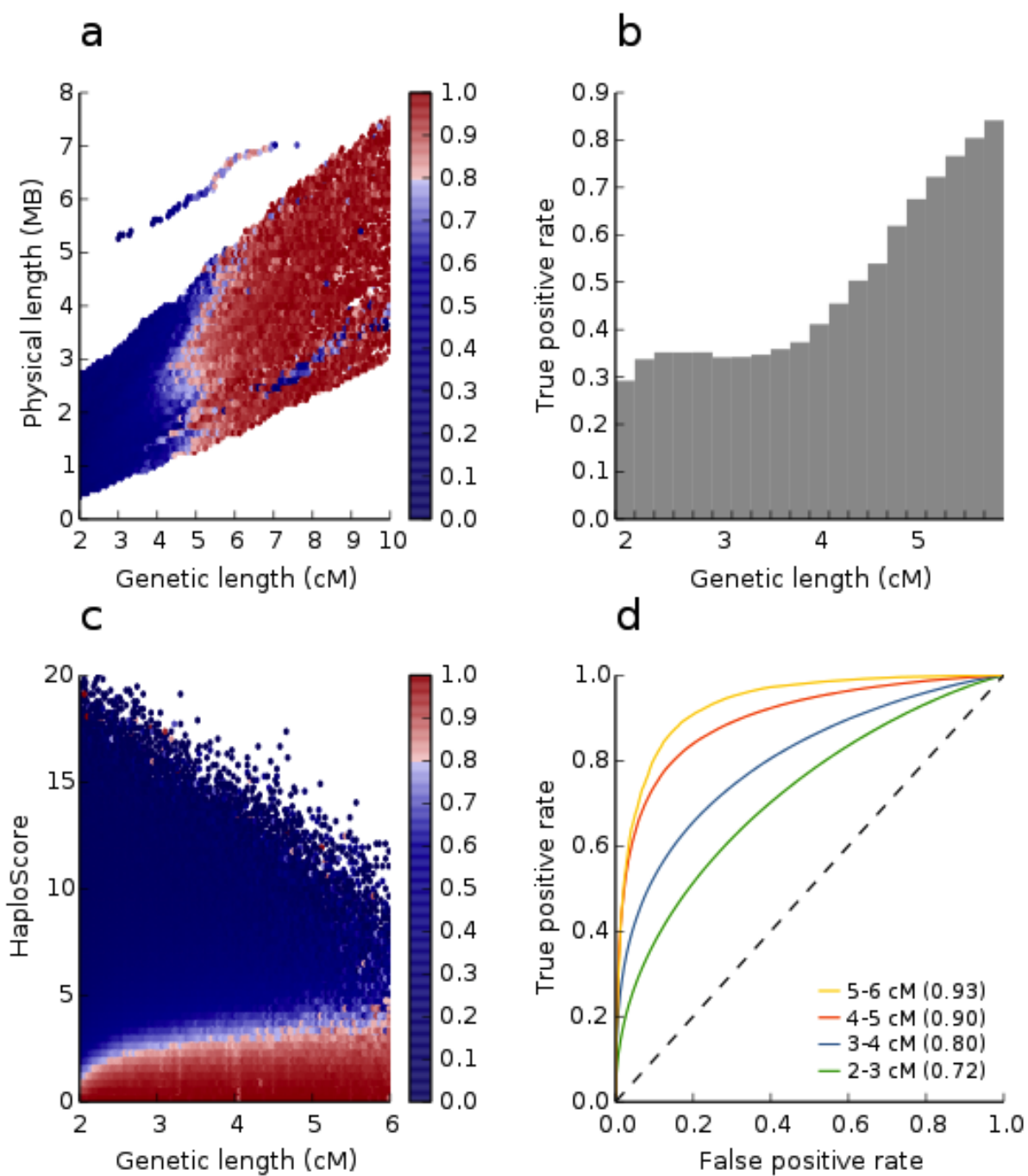
## Supplementary Figures



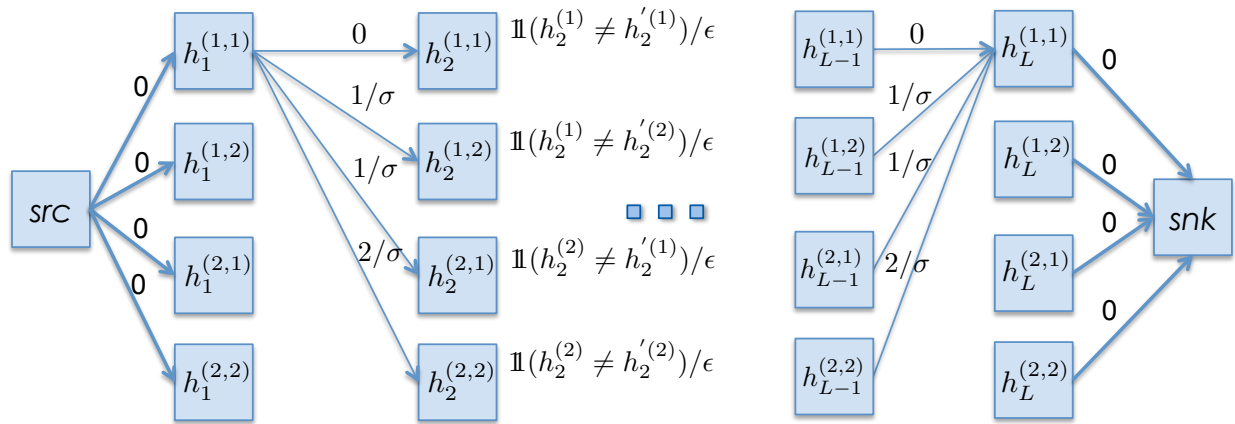
**Supplementary Figure 1:** Choosing the parent through which child-other IBD segments have been transmitted. The genome is represented as a horizontal gray line. Assayed sites compatible with IBD between the listed individual and a hypothetical other individual (not pictured) are indicated as vertical black lines. Assayed sites incompatible with IBD (e.g., opposite homozygote sites) are indicated as red crosses. Orange boxes indicate reported IBD segments between the listed individual and the hypothetical other individual (not pictured). **(a)** The unambiguous case in which one parent has a corresponding IBD segment and the other parent does not. Here, the father would be selected as the parent for analysis. **(b)** The case where each parent has an IBD segment that partially overlaps the child segment. The parent selected for analysis is determined by the fraction of sites shared IBD. In this case, despite the longer physical length of the father's segment, the mother would be selected since her segment overlap (5 of 9 sites) is larger than the father's (3 of 9 sites). **(c)** The case where neither parent has a reported IBD segment. The father would be selected as the parent for analysis, since his genotype contains fewer opposite homozygote sites in the child IBD region.



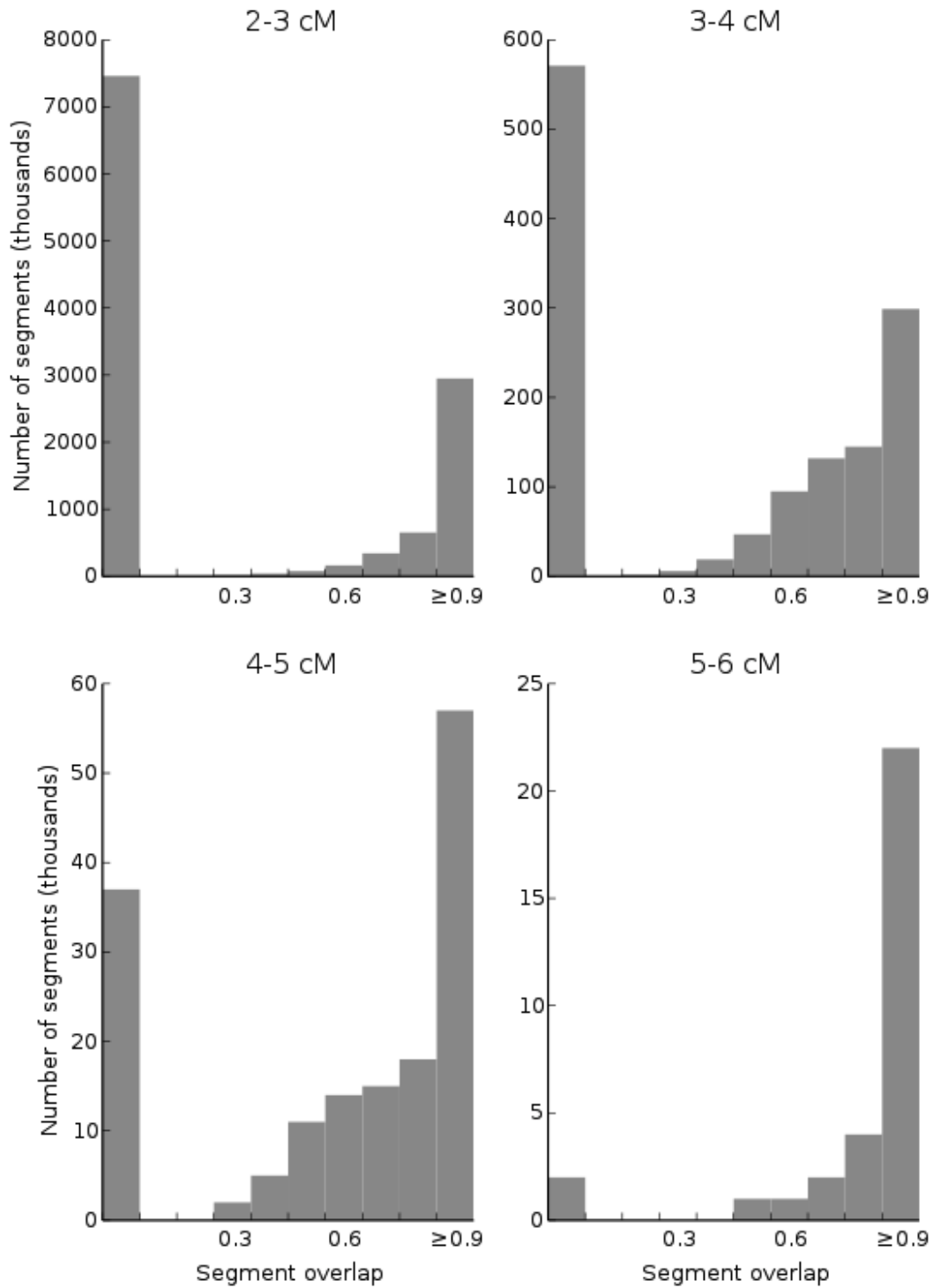
**Supplementary Figure 2:** Switch errors in BEAGLE-phased data occur at a nearly-constant rate across chromosomes. Switch error positions were detected in 2,952 trio children by comparing BEAGLE-phased haplotypes with trio-phased haplotypes and assuming trio-phased data was truth. The average individual switch error rate was calculated at each site by dividing the total number of switch errors at that site by 2,952. Red lines plot the cumulative switch error rate scaled by the number of sites on the chromosome, to facilitate inter-chromosomal comparison. Numbers in the top left of each graph indicate the average per-site switch error rate for the chromosome. Black dashed lines indicate the expected individual cumulative switch errors per site assuming a constant switch error rate at each site on the chromosome.



**Supplementary Figure 3:** IBD segment overlap and HaploScore performance on chromosome 21 using trio-phased trios. The figure is calculated in the same manner as **Fig. 2**, using trio-phased data for all 2,952 trios. The similarity of this figure and **Fig. 2** indicates that haplotype phasing errors do not contribute substantially to the estimates of IBD accuracy.

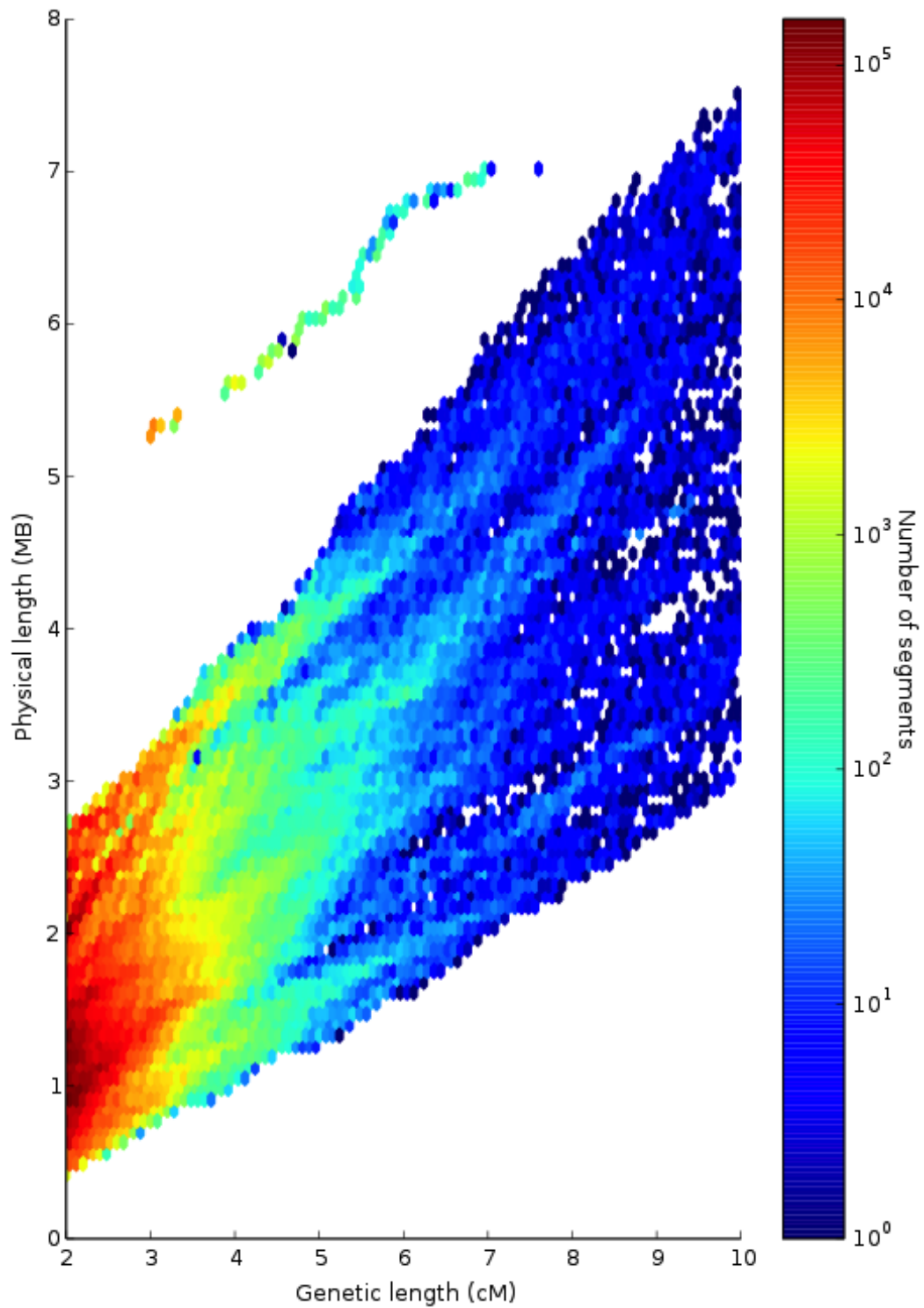


**Supplementary Figure 4:** Graph illustrating the HaploScore computation. The graph has one source, one sink and one level per genotyped site in the IBD segment. At each level  $l$ , the graph contains four nodes, indicating the haplotype configuration at site  $l$ . Each node has weight 0 if the two corresponding alleles are the same, or  $1/\epsilon$  if they are different. Each node at level  $l$  has four outgoing directed edges, one to each of the four nodes in level  $l + 1$ . The edge weights are 0,  $1/\sigma$ , or  $2/\sigma$ , depending on whether 0, 1 or 2 switch errors are necessary to explain the transition. For clarity, some edges are omitted in this figure. The source node  $src$  has four outgoing directed edges with weight 0, one to each of the four nodes in level 1. Each node in level  $L$  has one outgoing directed edge to the sink node  $snk$  with weight 0.

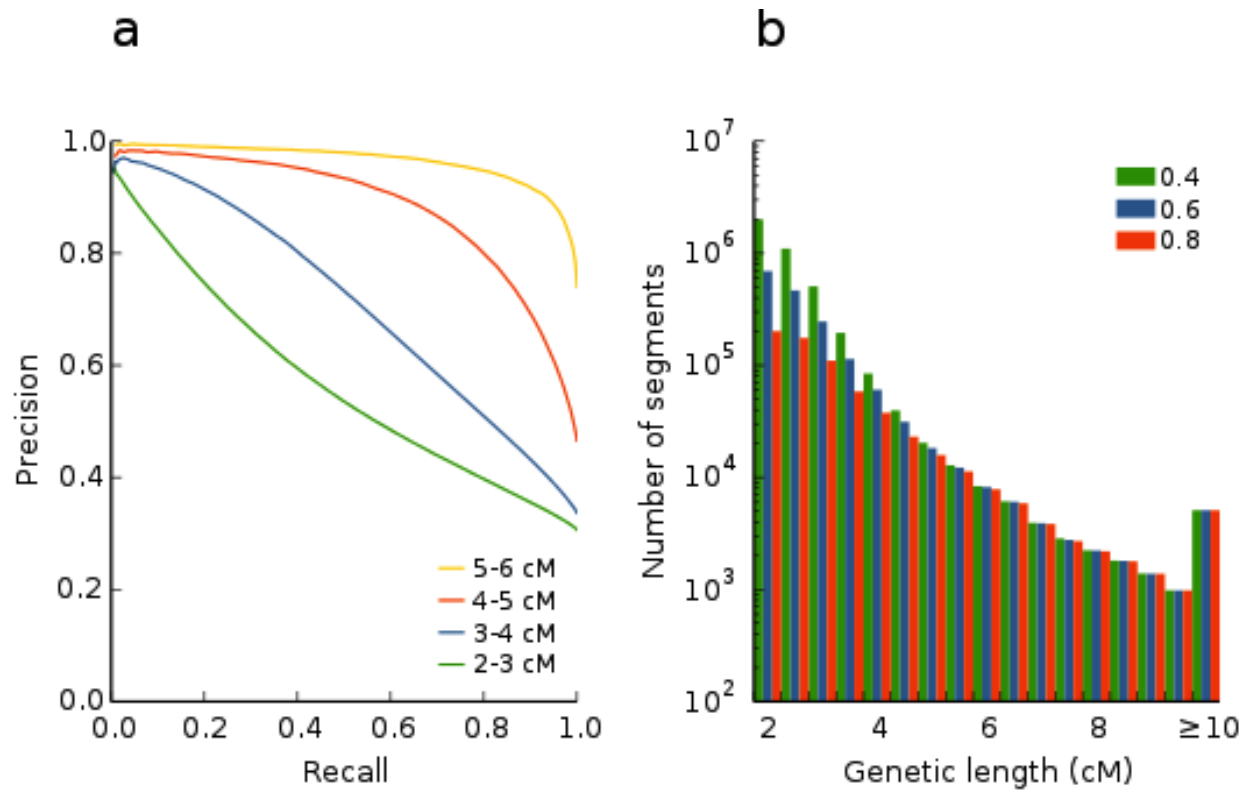


**Supplementary Figure 5:** Histograms of segment overlap in chromosome 21 child-other segments, displayed separately for four segment genetic length ranges. Shorter reported segments tend to have more segments with little to no corroborating parent-other segments. Note the scale changes on the y-axis: though the fraction of true segments of length  $< 3$  cM is smallest, this range contains roughly 10-fold more true segments than all other length ranges combined.

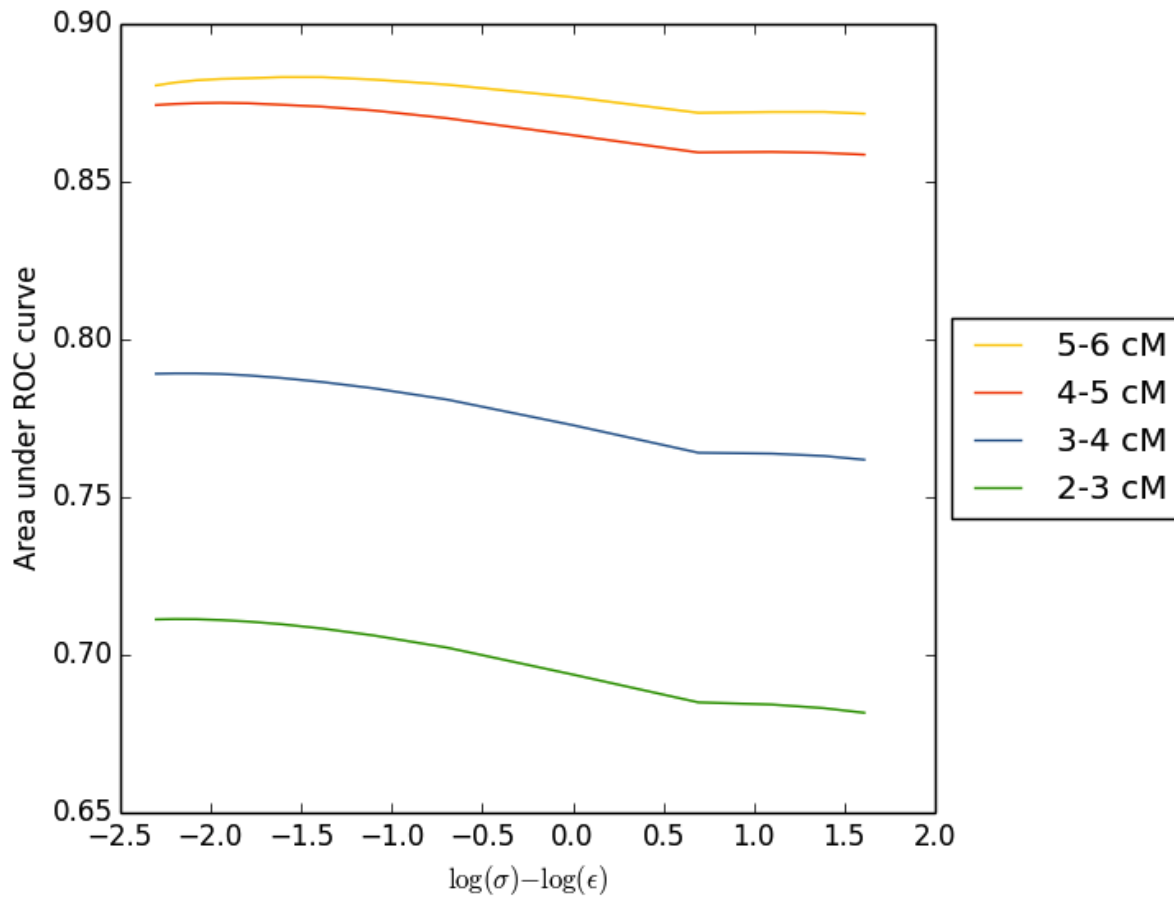




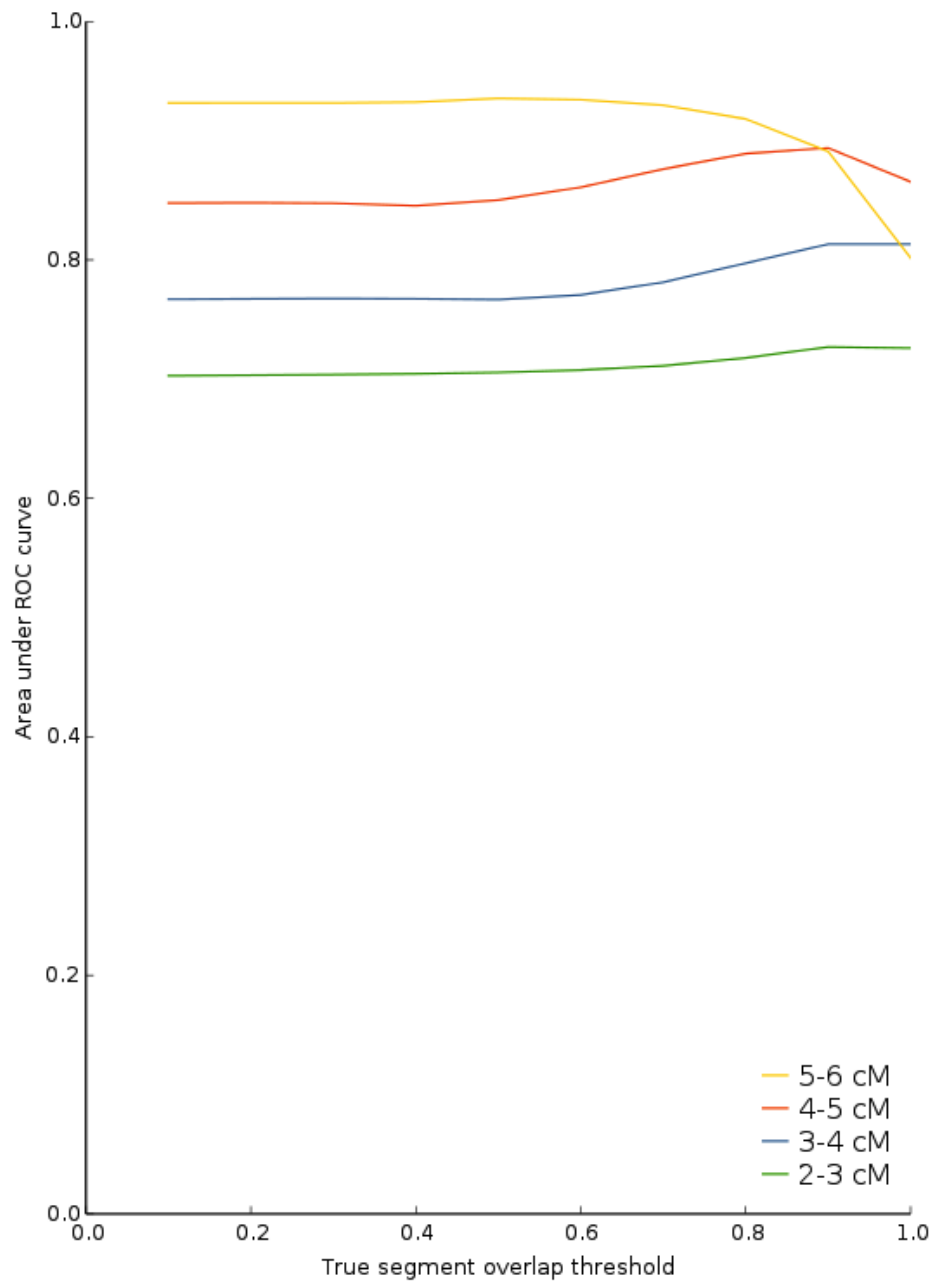
**Supplementary Figure 6:** Length distribution of child-other IBD segments. Heat map shows the number of segments in each bin segregating by the genetic and physical lengths of the segments. Axes identical to those in Fig. 2a.



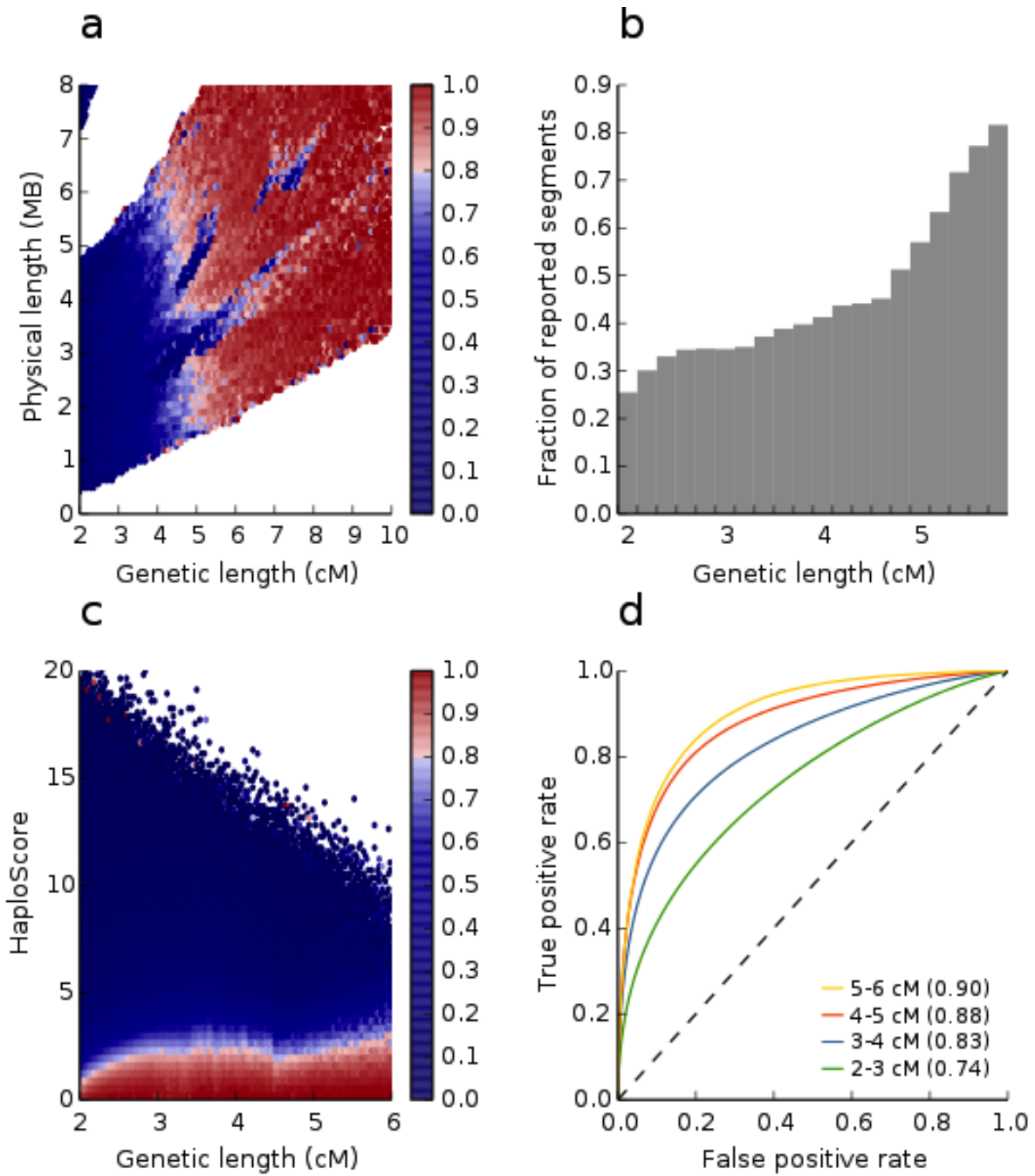
**Supplementary Figure 7:** Segment detection and HaploScore filtering results. **(a)** Precision-recall plot for child-other segments binned by segment length. **(b)** Histogram of number of segments reported after filtering at three different HaploScore thresholds,  $t \in \{0.4, 0.6, 0.8\}$ , as described above in **HaploScore filtering thresholds**. More stringent filtering parameters have the largest effect on short segments, which are most enriched for false positives (**Supplementary Fig. 5**). Note that the y-axis is on a log scale.



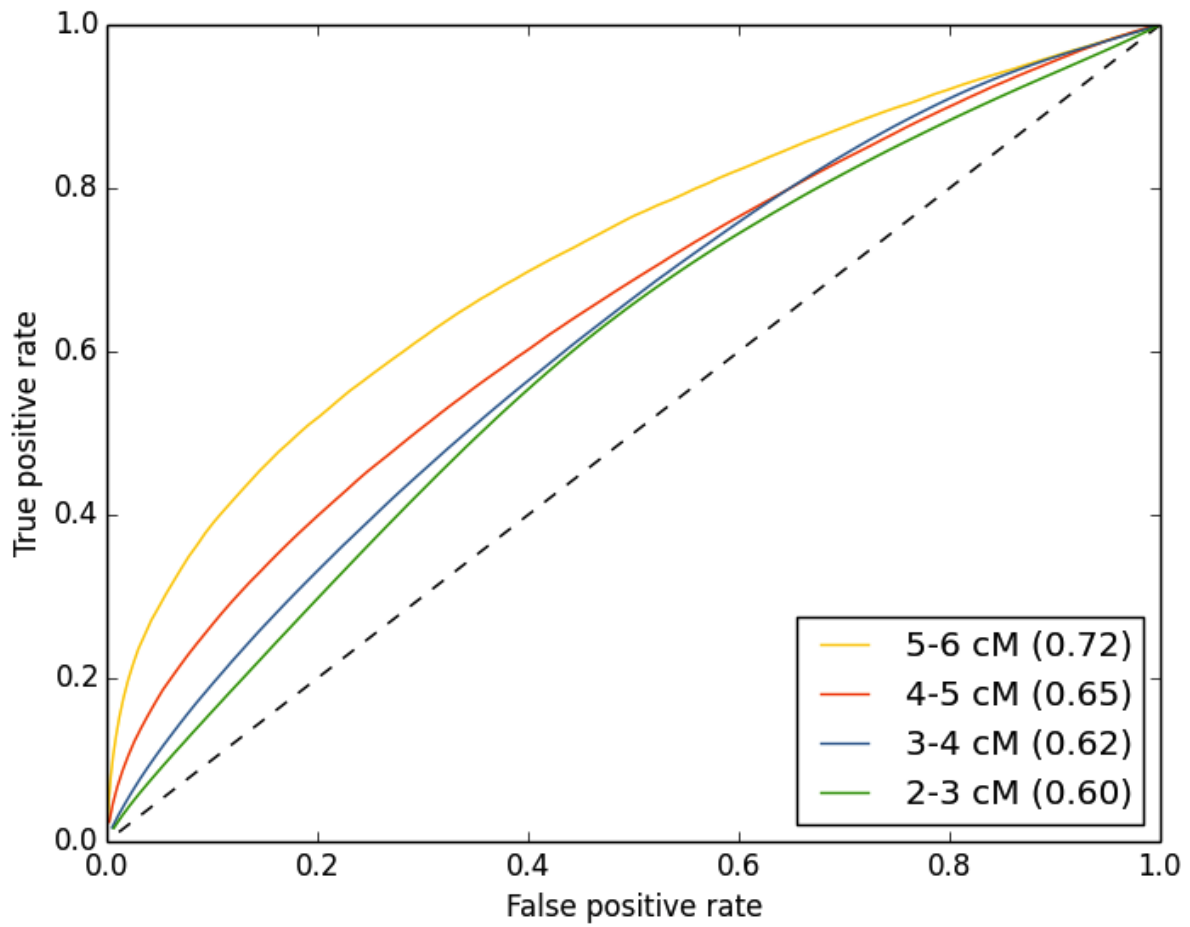
**Supplementary Figure 8:** HaploScore is robust to a wide parameterization of genotype and switch error rates. We varied the switch error rate  $\sigma$  relative to the genotyping error rate  $\epsilon$ . For each value of  $\sigma$ , we evaluated the resulting AUC discriminating by HaploScore, where we defined true positive segments as having a segment overlap of at least 0.80.



**Supplementary Figure 9:** HaploScore is robust to a wide parameterization of segment overlap required to classify a segment as a true positive. We classified true positive segments as those exceeding ten different segment overlap thresholds (0.1, 0.2, ..., 1.0) and calculated the resulting AUC discriminating by HaploScore.



**Supplementary Figure 10:** IBD segment overlap and HaploScore performance on chromosome 10. The figure is calculated in the same manner as **Fig. 2**.



**Supplementary Figure 11:** Receiver operating characteristic for reported IBD segments of various lengths, discriminating by LODscore. True positive IBD segments are defined as having at least 80% of their sites encompassed by a parent-other segment. The area under each curve is parenthesized in its legend entry.

## Supplementary Tables

**Supplementary Table 1:** Haplotype and diplotype window matches in child-other segments. **(a)** Counts of window types in windows contained within a corresponding parent-other segment. **(b)** Counts of window types in windows that are not contained within a corresponding parent-other segment.

**a**

	Child Diplo	Child Haplo	Child Both	<i>Total</i>
<b>Par None</b>	0	0	0	0
<b>Par Diplo</b>	6,283,300	56,393	1,045,425	7,385,118
<b>Par Haplo</b>	57,353	243,447	236,157	536,957
<b>Par Both</b>	1,098,359	243,490	13,733,586	15,075,435
<b><i>Total</i></b>	<i>7,439,012</i>	<i>543,330</i>	<i>15,015,168</i>	<i>22,997,510</i>

**b**

	Child Diplo	Child Haplo	Child Both	<i>Total</i>
<b>Par None</b>	14,055,602	483,921	5,853,193	20,392,716
<b>Par Diplo</b>	7,574,059	77,905	2,068,399	9,720,363
<b>Par Haplo</b>	82,378	243,698	372,885	698,961
<b>Par Both</b>	931,599	222,127	8,579,104	9,732,830
<b><i>Total</i></b>	<i>22,643,638</i>	<i>1,027,651</i>	<i>16,873,581</i>	<i>40,544,870</i>

Par, parent; Diplo, diplotype match only; Haplo, haplotype match only.

**Supplementary Table 2:** Genotype probabilities for a pair of individuals for different IBD states.  $p$  represents the allele frequency of allele A and  $q (= 1 - p)$  represents the allele frequency of allele B.

$(G_1, G_2)$	IBD0	IBD1	IBD2
AA, BB	$2p^2q^2$	0	0
AA, AA	$p^4$	$p^3$	$p^2$
AA, AB	$4p^3q$	$2p^2q$	0
AB, AB	$4p^2q^2$	$p^2q + pq^2$	$2pq$

**Supplementary Table 3:** Observed genotype probabilities with genotyping errors.

	$G_{true} = AA$	$G_{true} = AB$	$G_{true} = BB$
$G_{obs} = AA$	$(1 - \epsilon)^2$	$(1 - \epsilon)\epsilon$	$\epsilon^2$
$G_{obs} = AB$	$2(1 - \epsilon)\epsilon$	$(1 - \epsilon)^2 + \epsilon^2$	$2(1 - \epsilon)\epsilon$
$G_{obs} = BB$	$\epsilon^2$	$(1 - \epsilon)\epsilon$	$(1 - \epsilon)^2$

obs, observed.



## References

- [1] Kong, A. *et al.* Detection of sharing by descent, long-range phasing and haplotype imputation. *Nature Genetics* **40**, 1068–1075 (2008).
- [2] Krawitz, P. M. *et al.* Identity-by-descent filtering of exome sequence data identifies PIGV mutations in hyperphosphatasia mental retardation syndrome. *Nature Genetics* **42**, 827–829 (2010).
- [3] Jonsson, T. *et al.* A mutation in APP protects against Alzheimer’s disease and age-related cognitive decline. *Nature* **488**, 96–99 (2012).
- [4] Visscher, P. M. *et al.* Assumption-free estimation of heritability from genome-wide identity-by-descent sharing between full siblings. *PLOS Genetics* **2**, e41 (2006).
- [5] Zuk, O., Hechter, E., Sunyaev, S. R. & Lander, E. S. The mystery of missing heritability: genetic interactions create phantom heritability. *Proceedings of the National Academy of Sciences* **109**, 1193–1198 (2012).
- [6] Palamara, P. F., Lencz, T., Darvasi, A. & Peer, I. Length distributions of identity by descent reveal fine-scale demographic history. *The American Journal of Human Genetics* (2012).
- [7] Gusev, A. *et al.* The architecture of long-range haplotypes shared within and across populations. *Molecular Biology and Evolution* **29**, 473–486 (2012).
- [8] Ralph, P. & Coop, G. The geography of recent genetic ancestry across Europe. *PLOS Biology* **11**, e1001555 (2013).
- [9] Albrechtsen, A. *et al.* Relatedness mapping and tracts of relatedness for genome-wide data in the presence of linkage disequilibrium. *Genetic Epidemiology* **33**, 266–274 (2009).
- [10] Han, L. & Abney, M. Using identity by descent estimation with dense genotype data to detect positive selection. *European Journal of Human Genetics* (2012).
- [11] Browning, S. R. & Browning, B. L. Identity by descent between distant relatives: detection and applications. *Annual Review of Genetics* **46**, 617–633 (2012).
- [12] Browning, B. L. & Browning, S. R. Efficient multilocus association testing for whole genome association studies using localized haplotype clustering. *Genetic Epidemiology* **31**, 365–375 (2007).
- [13] Gusev, A. *et al.* Whole population, genome-wide mapping of hidden relatedness. *Genome Research* **19**, 318–326 (2009).
- [14] Browning, B. L. & Browning, S. R. Improving the accuracy and efficiency of identity-by-descent detection in population data. *Genetics* **194**, 459–471 (2013).
- [15] Fan, J.-B. *et al.* Highly parallel SNP genotyping. In *Cold Spring Harbor Symposia on Quantitative Biology*, vol. 68, 69–78 (Cold Spring Harbor Laboratory Press, 2003).
- [16] Hinds, D. A. *et al.* A genome-wide association meta-analysis of self-reported allergy identifies shared and allergy-specific susceptibility loci. *Nature Genetics* **45**, 907–911 (2013).
- [17] Henn, B. M. *et al.* Cryptic distant relatives are common in both isolated and cosmopolitan genetic samples. *PLOS ONE* **7**, e34267 (2012).
- [18] Browning, S. R. & Browning, B. L. Rapid and accurate haplotype phasing and missing-data inference for whole-genome association studies by use of localized haplotype clustering. *The American Journal of Human Genetics* **81**, 1084–1097 (2007).

- [19] Frazer, K. A. *et al.* A second generation human haplotype map of over 3.1 million SNPs. *Nature* **449**, 851–861 (2007).
- [20] Kent, W. J. *et al.* The human genome browser at UCSC. *Genome Research* **12**, 996–1006 (2002).
- [21] Paynter, R. A. *et al.* Accuracy of multiplexed Illumina platform-based single-nucleotide polymorphism genotyping compared between genomic and whole genome amplified DNA collected from multiple sources. *Cancer Epidemiology Biomarkers & Prevention* **15**, 2533–2536 (2006).